A Numerical Study on Metallic Powder Flow in Coaxial Laser Cladding

H. Liu[1,2†], J. B. Hao[1], G. Yu[3], H. F. Yang[1], L. W. Wang[4] and Z. T. Han[1]

[1] *School of Mechanical and Electrical Engineering, China University of Mining and Technology, Xuzhou, Jiangsu, 221116, China*
[2] *Jiangsu Key Laboratory of Mine Mechanical and Electrical Equipment, China University of Mining & Technology, Xuzhou, Jiangsu 221116, China*
[3] *Key Laboratory of Mechanics in Advanced Manufacturing, Institute of Mechanics, Chinese Academy of Science, Beijing, 100044, China*
[4] *School of Civil Engineering, Beijing Jiaotong University, Beijing, 100044, China*

†*Corresponding Author Email: liuhao56@cumt.edu.cn*

ABSTRACT

In coaxial laser cladding, the quality and property of deposition products are greatly influenced by the powder flow, which is responsible to transport additive materials to the deposition point on a substrate precisely. The metallic powder flow in coaxial laser cladding is simulated by a numerical model based on the gas-solid flow theory. The characteristics of powder concentration distribution between coaxial nozzle and deposition point for a kind of nickel based alloy powder are studied by the proposed model. The relationship between the process parameters and powder flow characteristics, such as focus distance from the nozzle exit and maximum powder concentration, is analyzed to optimize the powder feeding process. In addition, the influence of substrate with different surface shapes on the powder flow is investigated. The results can be used as a guideline for the location of the substrate and the selection of proper processing parameters for coaxial laser cladding.

Keywords: Coaxial laser cladding; Gas-solid flow; Powder concentration distribution; Substrate shape.

NOMENCLATURE

a_1, a_2, a_3	constants for spherical particles	Re	relative Reynolds number
$C_{1\varepsilon}, C_{2\varepsilon}$	empirical constants in k-ε model	S	sectional area of the nozzle inlet
C_D	drag coefficient	t_c	time for the particle to cross the vortex
C_L	time scale constant	u_i, u_j	i, j component of the gas velocity
C_μ	constant in the turbulent viscosity	u_{1P}, u_{2P}	particle velocity before and after collision
d_c	diameter of carrier gas inlet		
d_e	diameter of nozzle exit	u_{Pi}	i component of the particle velocity
d_i	diameter of inner gas inlet	u', v', w'	random velocity fluctuation
d_m	particle size constant	v	gas velocity at nozzle inlet
d_o	diameter of outer gas inlet	v_c	velocity of carrier gas flow at the nozzle inlet
d_p	particle diameter		
dt	time step	v_i	velocity of inner gas flow at the nozzle inlet
e_n	restitution coefficient		
F	powder feed rate	v_o	velocity of outer gas flow at the nozzle inlet
F_D	drag force per unit particle mass and unit velocity difference		
F_d	mass fraction of particles with diameter greater than d	w_m	width of middle annular channel
		w_o	width of outer annular channel
F_i	additional force per unit particle mass	x_i, x_j	position in i, j direction
G_b	generation of turbulence kinetic energy due to buoyancy	δ_{ij}	kronecker delta
		ε	dissipation of kinetic energy of turbulence
G_k	rate production of turbulence kinetic energy owing to the mean velocity gradient	ζ	normally distributed random number
		θ_m	angle of middle annular channel

g_i	component of the gravitational acceleration	θ_o	angle of outer annular channel
h	height below the nozzle exit	μ	molecular viscosity
k	kinetic energy of turbulence	μ_t	turbulent viscosity
L_e	vortex length scale	ρ	gas density
n	spread parameter	ρ_P	particle density
Pr_t	turbulent Prandtl number	$\sigma_k, \sigma_\varepsilon$	empirical constants in k-ε model
p	pressure	τ	particle relaxation time
Q	gas volume per unit time	τ_e	vortex life
		τ_{ij}	viscous stress

1. INTRODUCTION

In laser cladding process, a high-performance coating can be produced by adding metallic materials into a moving melt pool through sequential deposition tracks. Each track is created by rapid solidification of the melt pool that is formed by melting the additive materials and a thin layer of the substrate employing a laser beam. Combining with a computer-aided design model of an object, this technology can also be used to create a three-dimensional component by multi-layer deposition (Dinda *et al.* 2012). The additive material usually is in the form of metallic powder, which can be injected laterally or coaxially to the laser beam (Zekovic *et al.* 2007). Between the two different ways of powder feeding, coaxial laser cladding is easier to realize automation because of its independence from the direction of motion (Pinkerton and Li 2004).

The coaxial laser cladding process can be classified into three stages. In the first stage, metallic powder particles are delivered into the substrate by a carrier gas flow. Laser beam, powder flow, and gas flow interact with each other before these particles reach a substrate. In the second stage, laser energy is absorbed by the surface of the substrate, so a melt pool is formed by molten metal and the powder particles. When the substrate or the laser beam moves, the melt pool solidifies rapidly and then a thin layer is produced on the substrate surface in the third stage. The powder flow characteristics in the first stage of coaxial laser cladding, such as the powder focal distance and the maximum powder concentration, not only dominate the total mass of powder particles reached the melt pool, but also have a great influence on the laser power attenuation (Pinkerton 2007). The clad qualities are influenced by the powder concentration distribution between the coaxial nozzle and the substrate (Liu and Li 2005). Therefore, it is essential to study the powder flow characteristics to build a coating on substrate with accurate dimensions and high powder using efficiency.

The powder flow characteristics are determined by many factors, including the structure and the size of coaxial nozzle, shielding gas flow rate, carrier gas flow rate, powder feed rate, the properties of powder particles and environmental conditions. There are complex relationships between these input variables and the powder concentration distribution. Lin (2000) studied the focused and columnar powder streams of a coaxial nozzle with various arrangements of the nozzle exit, proving that the nozzle arrangements play a critical role in concentration mode of the powder flow. Pan and Liou (2005) presented a stochastic model considering powder particles shape effects to simulate the powder flow in the nozzle. They studied the effect of the width of the powder outlet passage on the powder flow shape. Yang (2009) developed a concentration model of powder particle stream for coaxial laser cladding, and found that the exit width of the coaxial nozzle had a positive relationship with powder stream diameter and a negative relationship with peak powder concentration at focus position. Tabernero *et al.* (2010) investigated the powder flux distribution evolution for three different kinds of metallic powder using a 3-D numerical model. Balu *et al.* (2012) conducted a parametric study on a coaxial multi-material powder flow, and measured some key powder flow characteristics, such as the stand-off distance, the diameter of the powder stream at the stand-off distance, and the velocity of the powder particles. Liu *et al.* (2015) studied the collision behavior of particles with the internal wall of a coaxial nozzle, and revealed the effect of powder properties on the powder flow through a gas-solid model.

However, process parameters such as shielding and carrier gas flow rate, powder feed rate, the shape of substrate, have barely discussed in those works. In this paper, a 3-D numerical model of metallic powder flow is developed based on a given coaxial nozzle, which has the ability to predict the powder concentration distribution, particle velocities and trajectories between the coaxial nozzle and the deposition point. The relationship between the gas flow rate and powder concentration distribution is investigated. Further, the effect of substrate on the powder flow is also discussed.

2. POWDER FLOW MODEL

2.1 Description and Assumptions

Laser cladding process and a typical coaxial nozzle is shown in Fig. 1. There are three different kind of gas flow in the coaxial nozzle. At the center, the gas flow is parallel to the laser beam and the main purpose of this inner gas flow is to protect the lenses from the hot powder particles that ricocheted from the substrate. Another kind of gas flow called carrier gas flow is to transport the powder particles to the deposition point. The outer gas flow generates protective atmosphere in peripheral of

powder flow to prevent powder particles from oxidation. All these gas flows and their interactions affect the powder concentration distribution below the exit of coaxial nozzle.
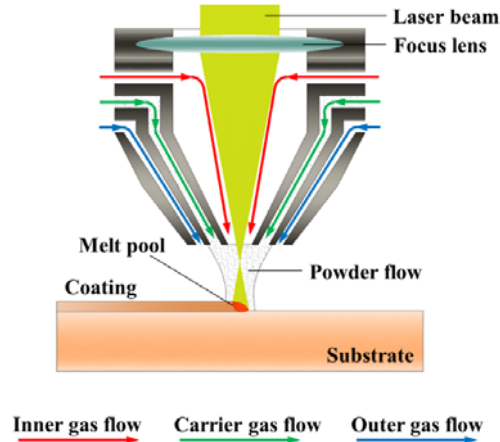

Inner gas flow   **Carrier gas flow**   **Outer gas flow**

Fig. 1. Sketch of laser cladding process and geometry structure of coaxial nozzle.

In the powder stream, shielding and carrier gas should be considered as continuous phase while powder particles should be treated as discrete phase into the continuous phase. Hence, the model of powder stream consists of two different modules. The proposed model is based on the following assumptions (Zekovic *et al.* 2007):

1. The gas flow is considered as a steady-state turbulent flow with constant velocity distribution at the inlet boundary. The initial velocities of powder particles are constant and perpendicular to the inlet surface of the nozzle.

2. The forces of drag, inertia and gravity are considered in the model, while other forces, including pressure and surrounding flow acceleration, are neglected.

3. The collision between particles is not considered, because the probability is too low.

4. The powder particles are spherical, and the particle size is assumed to follow the general Rossin-Rammler distribution expression.

5. Heat transfer by laser radiation is neglected.

6. Powder particles flow represented as a discrete phase does not affect the continuous phase due to the low mass and concentration of the particles.

2.2 Continuous Phase Modeling

The continuous phase modeling is based on Navier-Stokes differential equations with the Reynolds method of averaging time-dependent equations, together with the standard k-ε turbulent model. Since the gas flow is considered to be steady, incompressible, isothermal and chemically homogeneous, the time-averaged, governing equations for turbulent flow are expressed as follows (Zhao *et al.* 2015).

Conservation of mass:

$$\frac{\partial}{\partial x_i}(\rho u_i) = 0 \tag{1}$$

where ρ is gas density, and the vectors u_i and x_i represent the velocity and position in i direction.

Conservation of momentum:

$$\frac{\partial}{\partial x_j}(\rho u_i u_j) = -\frac{\partial p}{\partial x_i} + \frac{\partial \tau_{ij}}{\partial x_j} + \rho g_i \tag{2}$$

where p, g_i and τ_{ij} is pressure, gravitational acceleration, viscous stress tensor, respectively. The τ_{ij} is given by

$$\tau_{ij} = [(\mu + \mu_t)(\frac{\partial u_i}{\partial x_j} + \frac{\partial u_j}{\partial x_i})] - \frac{2}{3}\mu_t \frac{\partial u_i}{\partial x_i}\delta_{ij} \tag{3}$$

where μ is the molecular viscosity, δ_{ij} is the Kronecker delta that δ_{ij}=1 for i=j, otherwise δ_{ij}=0, and μ_t is the turbulent viscosity defined by

$$\mu_t = \rho C_\mu \frac{k^2}{\varepsilon} \tag{4}$$

where C_μ=0.09 is a constant, k the kinetic energy of turbulence, and ε the dissipation of kinetic energy of turbulence, which is defined in standard k-ε turbulent model as follows:

Conservation of kinetic energy of turbulence:

$$\frac{\partial}{\partial x_i}(\rho u_i k) = \frac{\partial}{\partial x_i}(\frac{\mu_t}{\sigma_k}\frac{\partial k}{\partial x_i}) + G_k + G_b - \rho\varepsilon \tag{5}$$

Conservation of dissipation of kinetic energy of turbulence:

$$\frac{\partial}{\partial x_i}(\rho u_i \varepsilon) = \frac{\partial}{\partial x_i}(\frac{\mu_t}{\sigma_\varepsilon}\frac{\partial \varepsilon}{\partial x_i}) + C_{1\varepsilon}\frac{\varepsilon}{k}(G_k + G_b) - C_{2\varepsilon}\rho\frac{\varepsilon^2}{k} \tag{6}$$

$$G_k = \mu_t(\frac{\partial u_j}{\partial x_i} + \frac{\partial u_i}{\partial x_j})\frac{\partial u_i}{\partial x_j} \tag{7}$$

$$G_b = -g_i \frac{u_t}{\rho \, \mathrm{Pr}_t}\frac{\partial \rho}{\partial x_i} \tag{8}$$

where $C_{1\varepsilon}$=1.44, $C_{2\varepsilon}$=1.92, σ_k=1.0 and σ_ε=1.3 are empirical constants, Pr_t is the turbulent Prandtl number, G_k is the rate production of turbulence kinetic energy owing to the mean velocity gradients, G_b is the generation of turbulence kinetic energy due to buoyancy (Tabernero *et al.* 2010).

Standard wall functions are employed for the turbulent model, considering the low gas viscosity and the relatively low Reynolds number of the powder flow in the laser cladding. There is no need to refine the grids near the wall in the model using standard wall functions, which associate the physical quantities in the wall with these in the turbulent core. Thus a high calculation efficiency with sufficient accuracy is acquired.

2.3 Discrete Phase Modeling

In this study, powder particles as a discrete phase are considered to be dispersed in the gas flow, whose governing equations are given in the

standard fluid dynamics above. The trajectory of each powder particle is described in a Lagrangian reference frame based on a force balance that is written as:

$$\frac{du_{Pi}}{dt} = F_D(u_i - u_{Pi}) + \frac{(\rho_P - \rho)g_i}{\rho_P} + F_i \qquad (9)$$

where u_{Pi} is the velocity of particle, ρ_P is the particle density, and $F_D(u_i - u_{Pi})$ represents the drag force per unit particle mass expressed as:

$$F_D = \frac{18\mu}{\rho_P d_P^2} \frac{C_D \, \text{Re}}{24} \qquad (10)$$

where d_P is the particle diameter, Re is relative Reynolds number given by

$$\text{Re} = \frac{\rho d_P |u_i - u_{Pi}|}{\mu} \qquad (11)$$

and C_D is the drag coefficient that can be calculated as:

$$C_D = a_1 + \frac{a_2}{\text{Re}} + \frac{a_3}{\text{Re}^2} \qquad (12)$$

where a_1, a_2, a_3 are constants within a certain range of relative Reynolds number for spherical particles, see Morsi and Alexander. (1972).

Rosin-Rammler distribution is used to represent the size distribution of powder particles. In this method, the whole range of particle sizes is divided into a number of discrete intervals. Each of these intervals is described by a mean diameter d for trajectory calculations. According to Rosin-Rammler distribution, the mass fraction of particles with diameter greater than d is expressed by:

$$F_d = \exp(-(\frac{d}{d_m})^n) \qquad (13)$$

where d_m is the particle size constant, and n is the spread parameter.

The effect of velocity fluctuation on the particle in the turbulence flow is considered for particle trajectory calculation by the discrete random walk model. The turbulence is modeled by eddies defined by a Gaussian distributed random velocity fluctuation u', v', w' and a vortex life τ_e:

$$u' = v' = w' = \zeta \sqrt{\frac{2k}{3}} \qquad (14)$$

$$\tau_e = 2C_L \frac{k}{\varepsilon} \qquad (15)$$

where ζ is a normally distributed random number used for the three directions due to the assumption of isotropic turbulence, and C_L is the time scale constant.

The time for the particle to cross the vortex t_c can be calculated as:

$$t_c = -\tau \ln\left[1 - \left(\frac{L_e}{\tau|u - u_P|}\right)\right] \qquad (16)$$

where τ is the particle relaxation time, L_e is the vortex length scale, and $|u-u_P|$ is the magnitude of the relative velocity.

The particle is considered to interact with the fluid phase vortex over the smaller one among the vortex life τ_e and the crossing time t_c. When this time is reached, a new value of instantaneous velocity is obtained by using a new value of ζ in Eq.(14).

With the time integral of the force balance differential equation, the particle velocity at each point along its trajectory is obtained. The particle trajectory can be predicted by the kinematic equation as follow:

$$\frac{dx_i}{dt} = u_{pi} \qquad (17)$$

where x_i represents the position of the particle.

The collision between the particles and the internal wall of the coaxial nozzle is considered in this model. The restitution coefficient is used to evaluate the momentum loss of particle collision with the internal wall:

$$e_n = \frac{u_{2P}}{u_{1P}} \qquad (18)$$

where e_n is the restitution coefficient, and u_{1P}, u_{2P} is the particle velocity before and after collision. Generally, the restitution coefficient depends on the powder and nozzle material, impact velocity, hardness ratio, nozzle wall roughness. In this study, the restitution coefficient is considered as a constant when the material of coaxial nozzle and powder are selected to simplify the model.

The continuous phase is considered as a continuous homogeneous medium and solved by Navier-Stokes equations for each time step. The discrete phase is simulated by tracing a great quantity of particles in the calculated fluid field. The mass, momentum and energy in this discrete phase can be exchanged with the fluid phase.

2.4 Model Description

The solution technique used in this study is based on the FLUENT software, which solves the governing equations of continuous phase and discrete phase listed above by a specified finite-volume method. In order to explore the complete powder feeding process, a 3D geometry model of the whole coaxial nozzle together with the cylindrical space below the exit of nozzle as computational domain is built (Fig. 2). The geometry model has four carrier gas and powder particle inlets, and those four carrier gas path connect with an annular channel. The inner shielding gas inlet is located above the exit of the nozzle. There are two outer shielding gas inlets that deliver gas into the outer annular channel. The main structural parameters of the computational domain are listed in Table 1.
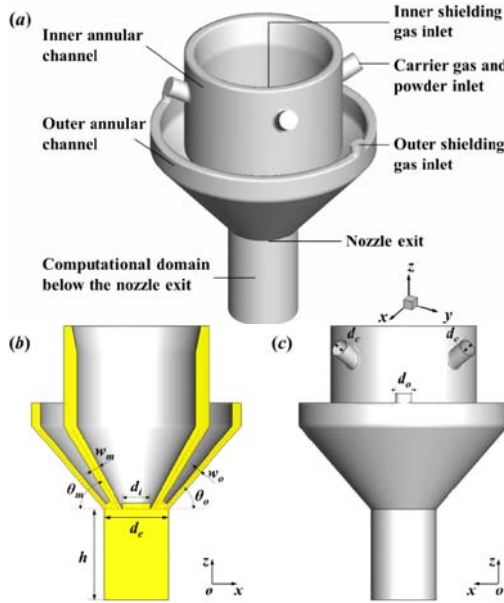
Fig. 2. The geometry model of the computational domain. (a) isometric view; (b) sectional view; (c) back view.

Table 1 Main structural parameters of the computational domain

Structural parameters	Symbol	Value
Inner gas inlet diameter (mm)	d_i	6
Carrier gas inlet diameter (mm)	d_c	4
Outer gas inlet diameter (mm)	d_o	2
Middle channel width (mm)	w_m	2.2
Middle channel angle (°)	θ_m	60
Outer channel width (mm)	w_o	1.2
Outer channel angle (°)	θ_o	50
Nozzle exit diameter (mm)	d_e	14.2
Height below the nozzle (mm)	h	20

The mesh is built in the basis of the 3-D geometry using GAMBIT software. Since the geometry is complex, the body fitted coordinate (BFC) grid system, which allows the non-standard geometry of the coaxial nozzle to be mapped into Cartesian or cylindrical geometry, is used to accurately predict the structure of the powder flow. The grid independency is performed for the simulation cases in this study. The mean element size is selected in the range of 0.3 mm to 1.0 mm with a step size of 0.5 mm. The results show that the powder concentration distribution is independent with the element density when the mean element size is less than 0.75 mm. Therefore, a mean element size of 0.7 mm is used considering computational efficiency. In this situation, there are 256044 elements for a 16.14 cm^3 domain of Fig. 2.

The representative cases in the coaxial laser cladding are free gas-solid flow and gas-solid flow at the start of the deposition on the substrate with various shapes. The boundary conditions of the free gas flow are shown in Fig. 3. Metallic powder is delivered by gas flow at a carrier gas velocity v_c. The inner shielding gas flows from the inlet at a

velocity v_i, and outer shielding gas at a velocity v_o (Fig. 3). The three kinds of gas inlet surface are defined as velocity inlet boundary condition, and the computational domain of coaxial nozzle is bounded by the wall boundary condition. The cylindrical computational domain below the nozzle, which has 20 mm in height and 14.2 mm in diameter, is large enough to capture gas-solid flow characteristics of interest, and defined as pressure outlet boundary condition at the side and the bottom surface.
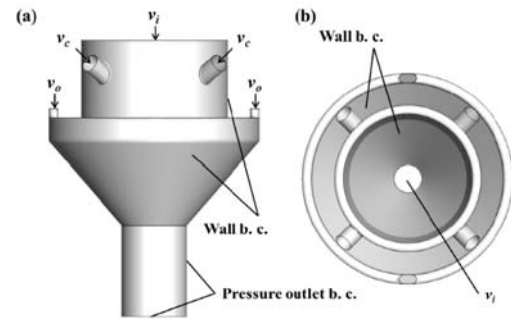

Fig. 3. Boundary conditions of the free gas flow. (a) front view; (b) vertical view.

The boundary conditions of the gas-solid flow at the start of the deposition on the substrate with various shapes are shown in Fig. 4. The coaxial nozzle geometry and the boundary conditions on it are the same as the case of free gas-solid flow. The geometry of the computational domain below the nozzle exit is modified according to the substrate shape. The wall boundary condition is defined at the bottom surface of the computational domain. For the cases with different substrate shape, the distance from the center of the nozzle exit to the deposition point on the substrate is set as a constant of 10 mm, so as to detect the powder flow variation.
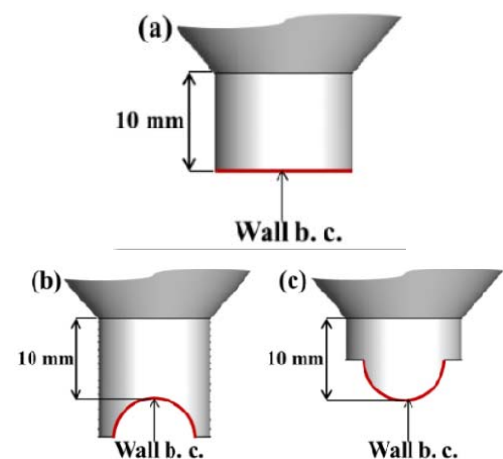

Fig. 4. Boundary conditions of the gas-solid flow with various substrates. (a) flat surface; (b) convex surface; (c) concave surface.

The gas velocities at the coaxial nozzle inlets are input parameters of the gas-solid model, while gas flow rates are processing parameters in laser

cladding experiments. To relate the experimental process parameters with numerical computation, the following equation is used:

$$v = \frac{Q}{S} \tag{18}$$

where v is the gas velocity at nozzle inlet, Q is the gas volume per unit time, and S is the sectional area of the nozzle inlet. The input parameters used in this study are summarized in Table 2.

Table 2 Input parameters of the simulations

Input parameters	Value
F (g/min)	1.75, 2.95, 4.15, 5.35, 6.55
v_i (m/s)	9, 2.5, 5, 7.5, 10
v_c (m/s)	1, 3, 5, 7, 9
v_o (m/s)	9, 2.5, 5, 7.5, 10

The carrier gas and shielding gas used in this study is argon, and the powder is nickel based alloy powder with a powder size distribution of 45 μm - 130 μm diameter. The particle size distribution of the powder is measured by sieve analysis. The measured and the approximated particle size distribution are shown in Fig. 5. The property parameters of the powder that are used in the simulations are listed in Table 3.
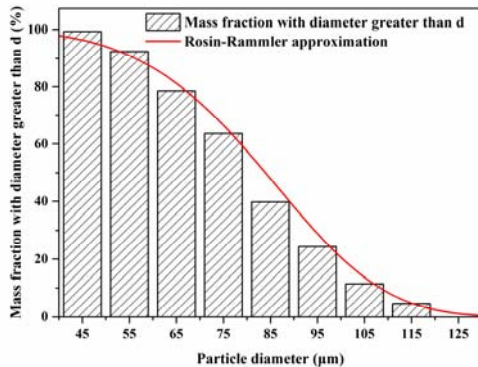
Fig. 5. The measured and assumed particle size distribution of nickel based alloy powder.

Table 3 Basic simulation parameters of particle phase

Parameters of particle pahse	Value
Density (kg/m³)	8350
Minimum diameter (μm)	40
Maximum diameter (μm)	130
Mean diameter (μm)	90
Number of discrete intervals	9
Spread parameter	4.7
Restitution coefficient	0.9
Gravity acceleration (m/s²)	-9.8

3. RESULTS AND DISCUSSION

3.1 Characteristics of Powder Flow

The proposed gas-solid model of the coaxial nozzle was validated by our previous work (Liu *et al*. 2015). In laser cladding, the powder flow below the nozzle plays an important role in the clad quality. Fig. 6 shows powder concentration distribution below the nozzle simulated by the model when the inner shielding gas and outer shielding gas is at velocity of 5 m/s, carrier gas is at velocity of 1 m/s at the inlets and powder feed rate is 4.1 g/min. The powder flow is annular when it is delivered from the coaxial nozzle. The powder flow converges below the coaxial nozzle tip under the effect of shielding gas and inertia of particles, generating an ellipsoidal high concentration zone. After the powder flow merged, it gradually diverges.
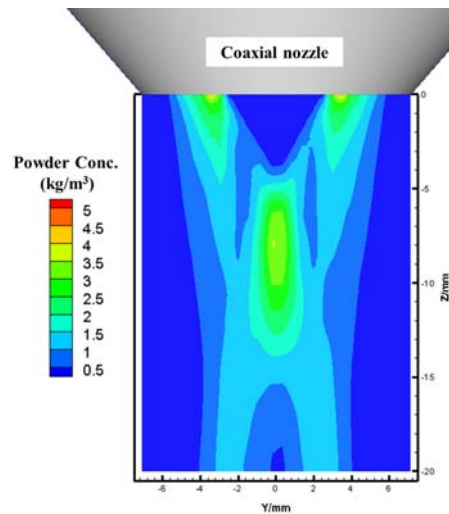

Fig. 6. Powder concentration distribution below the coaxial nozzle in longitudinal section.

To obtain more information about the powder flow, powder concentration at different horizontal planes below the coaxial nozzle is shown in Fig. 7. The Z coordinate values of these planes are 2.5 mm, 8 mm, 15 mm and 18 mm, respectively. The powder flow below the coaxial nozzle tip can be classified into three different zones based on the powder concentration distribution: annular zone, consolidation zone and dispersed zone.

The annular zone is just below the exit of nozzle (Fig. 7 (a)), and the powder concentration in the center increases with the standoff distance increasing in this zone. In the consolidation zone, the powder concentration is highest at the center of the horizontal plane (Fig. 7 (b)(c)), and it is located in the range of 4 mm to 15 mm away from the nozzle exit. The powder particles disperse from the center under the consolidation zone, so the dispersed zone is formed, the powder distribution of which is similar to that of the annular zone (Fig. 7(d)). Obviously, the substrate should be placed in the consolidation zone to improve powder efficiency and clad quality in laser cladding. As is seen in Fig. 7 (b) and (c), the powder concentration in the consolidation zone is approximately symmetrical, which is the reason that coaxial laser cladding is independent from motion direction.
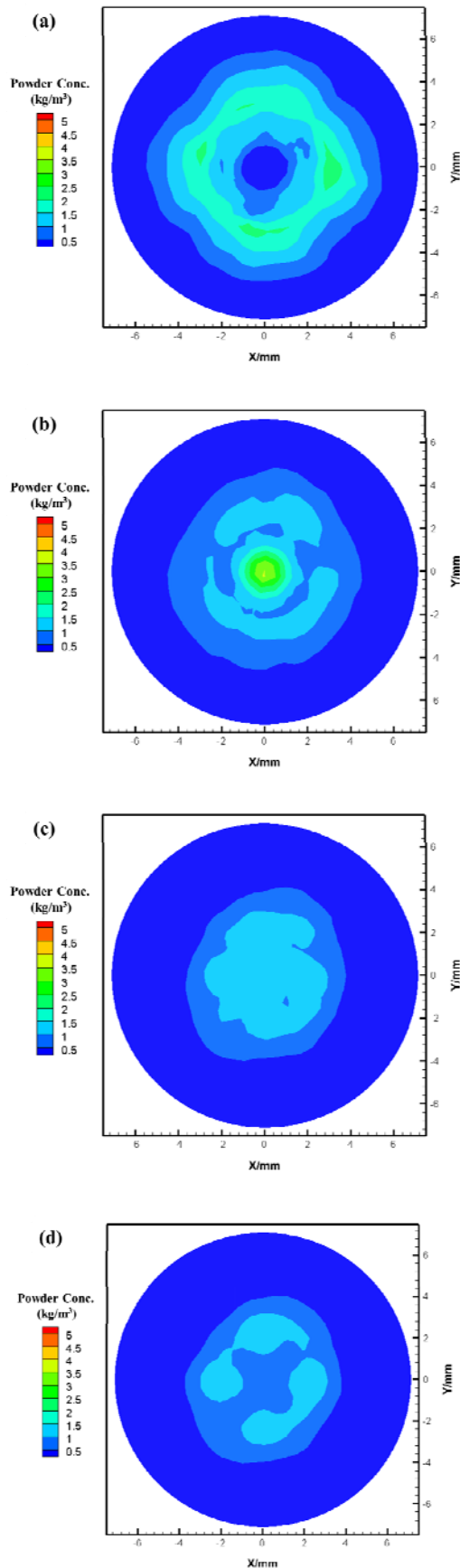
(a)

(b)

(c)

(d)

Fig. 7. Powder concentration distribution in transverse section with nozzle exit displacement of (a) 2.5 mm, (b) 8 mm, (c) 15 mm, and (d) 18 mm.

The plane where the powder concentration reaches its maximum is defined as focal plane, which is located 7.9 mm below the exit of coaxial nozzle in this case. Fig. 8 shows the powder concentration profiles along the nozzle axis and the radial axis in the focal plane, respectively. The powder concentration along the nozzle axis shows a rise first followed by a decline, and the peak powder concentration is about 3.5 kg/m³ in focal plane (Fig. 8 (a)). In the focal plane, it also can be seen that the powder concentration decreases rapidly from 3.5 kg/m³ to 1.0 kg/m³ within 2 mm of the nozzle axis, presenting a Gaussian or near-Gaussian shape. This downward trend slows down when it is 2 mm to 3mm away from nozzle axis (Fig. 8 (b)).

(a)

(b)
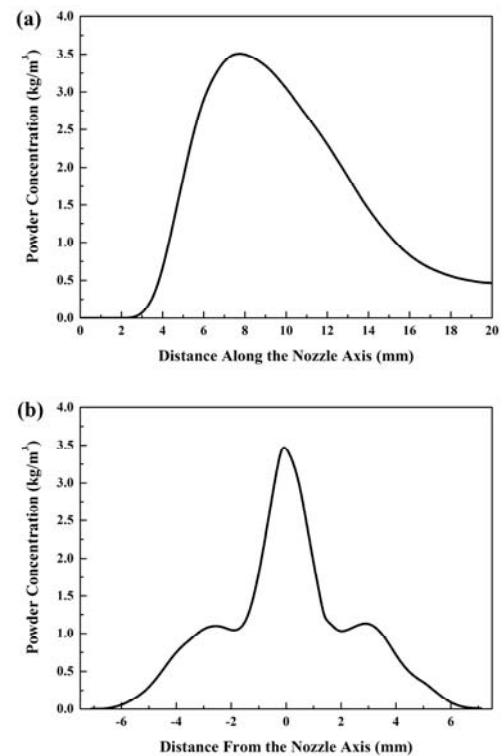
Fig. 8. Powder concentration profiles (a) along the nozzle axis and (b) the radial axis in the focal plane.

3.2 Effect of Process Parameters

The numerical results are summarized with variations of inner shielding gas rate, carrier gas rate, outer shielding gas rate and powder feed rate. The inner shielding gas rate plays an important role in powder flow convergence (Fig. 9). The powder concentration reaches its highest value of 6.6 kg/m³ at the distance of 3.9 mm away from the nozzle exit when the inner shielding gas is not used. With the inner shielding gas rate increasing, the powder focal distance from nozzle exit increases and the maximum powder concentration decreases. It becomes more difficult for powder flow to converge with higher inner gas flow rate. But the focus of powder flow could be controlled with the inner shielding gas flow. Considering the main purpose of inner shielding gas is to prevent

powder particles from rebounding to the nozzle, inner gas shielding rate should remain in a relatively moderate range.
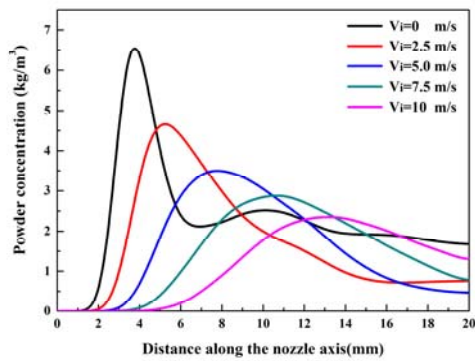

Fig. 9. Powder concentration along the nozzle axis with various inner shielding gas rate when carrier gas rate is 1m/s, outer shielding gas rate is 5m/s, and powder feed rate is 4.1g/min.

The effect of outer shielding gas on the powder flow is shown in Fig. 10. The maximum concentration of powder flow is only about 2.5 kg/m³ without the help of outer shielding gas flow. The powder concentration profiles are identical when the outer gas flow rate is in the range of 2.5 m/s to 10 m/s, with the maximum concentration increasing to about 3.5 kg/m³. It also can be seen from Fig. 10 that the outer gas flow does not have any influence on the focus of the powder flow. This result demonstrates that the outer gas flow could improve the maximum concentration of powder flow without altering its focus. However, this improvement is limited.
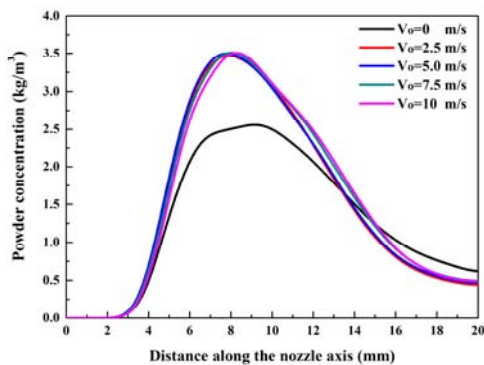

Fig. 10. Powder concentration along the nozzle axis with various outer shielding gas rate when carrier gas rate is 1m/s, inner shielding gas rate is 5m/s, and powder feed rate is 4.1g/min.

The influence of carrier gas on the powder flow is shown in Fig. 11. By increasing the carrier gas rate from 1 m/s to 5 m/s, the powder flow focal distance decreases from 7.9 mm to 4.9 mm. However, the focus of powder flow stays the same with the carrier gas flow rate in the range of 5 m/s to 9 m/s. Meanwhile, the maximum powder concentration has a remarkable downward trend

especially when the carrier gas rate increases from 3 m/s to 5 m/s. The decrease of the maximum powder concentration could be explained by a higher particle velocity, which makes the powder particle scatter under the nozzle exit. This indicates that good convergence characteristics of powder flow, which are suitable for coaxial laser cladding, can be obtained at a relatively low flow rate of carrier gas.
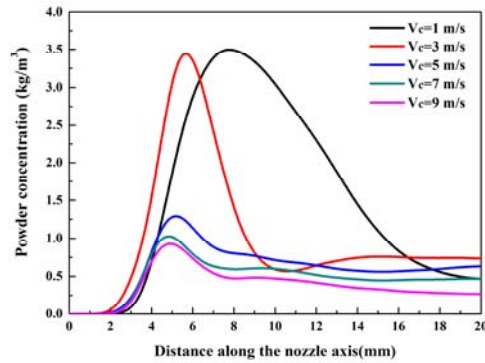

Fig. 11. Powder concentration along the nozzle axis with various carrier gas rate when inner shielding gas rate is 5m/s, outer shielding gas rate is 5m/s, and powder feed rate is 4.1g/min.

The powder concentration profiles along the nozzle axis under different powder feed rates are shown in Fig. 12. The focus of the powder flow is 7.9 mm at any powder feed rate. When the powder is transported at 1.75 g/min, 2.95 g/min, 4.15 g/min, 5.35 g/min, 6.55 g/min, the maximum concentration of powder flow is 1.5 kg/m³, 2.6 kg/m³, 3.5 kg/m³, 4.4 kg/m³, 5.4 kg/m³, respectively. Thus a strong positive linear relationship between the maximum powder concentration and the powder feed rate is detected. This is because the solid phase has little influence on the gas flow due to its low volume fraction during the laser cladding process. It could be deduced that a certain range of powder feed rate could be used at a proper combination of shielding gas flow and carrier gas flow, and the focus of powder flow is guaranteed.
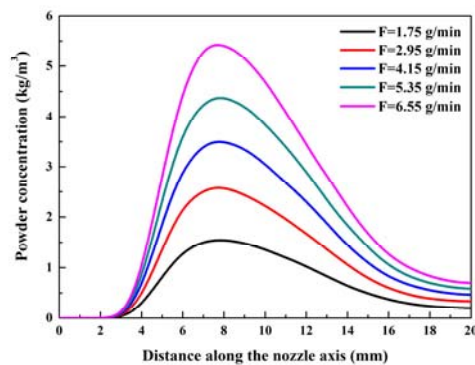

Fig. 12. Powder concentration along the nozzle axis with various powder feed rate when inner shielding gas rate is 5m/s, carrier gas rate is 1m/s, and outer shielding gas rate is 5m/s.

3.3 Effect of Substrate

In this study, a case of flat substrate placed 10 mm under the coaxial nozzle is discussed first. The location of the substrate is determined by the calculation results described above. The powder concentration distribution with the flat substrate is shown in Fig. 13. Comparing to the result without a substrate, the powder concentration above the substrate increases more than two times. This can be explained by two reasons. One is that a high-pressure and low-velocity gas mass is formed in the center due to the blocking effect of the substrate, which makes the powder particles decelerate and the number of particles increases in that space under a steady state of powder feeding process. The other is that particles hit the substrate and bounce into the calculation domain. Most of the particles in the center have much lower radial velocity than their axial velocity when they hit the substrate, so usually they rebound from the substrate many times within the center space (Fig.13(b)), which is a great contribution to the concentration of powder flow.
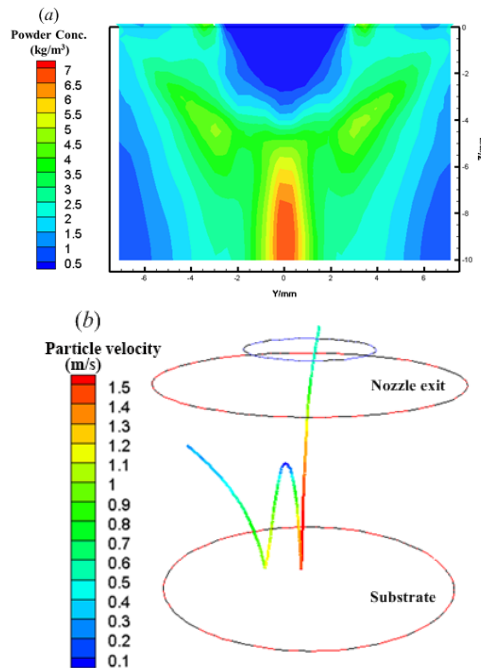

Fig. 13. The effect of flat substrate on the powder flow: (a) the powder concentration distribution below the coaxial nozzle; (b) rebound of a particle on the substrate.

Substrate with cylindrical surface, as well as flat surface, is also used in laser cladding. The powder concentration distribution with cylindrical surface is shown in Fig. 14 under two cases: convex surface and concave surface with radius of 5 mm. In order to compare with the result with flat substrate, the same powder feeding process parameters is applied and the distance from the nozzle exit to the substrate surface remains 10 mm. It can be seen that the powder concentration with convex surface is smaller than the result with flat surface as a whole. The gas flow downward along the convex surface makes the influence of the high-pressure and low-

velocity gas mass weaker so that the high powder concentration zone becomes smaller. On the contrary, the concave surface leads to the role of high-pressure and low-velocity gas mass stronger in the powder convergence. On the other side, particles can rebound within the space more times on the concave surface than on the convex surface. As a result, powder concentration with the concave surface is much greater near the surface as is shown in Fig. 14.
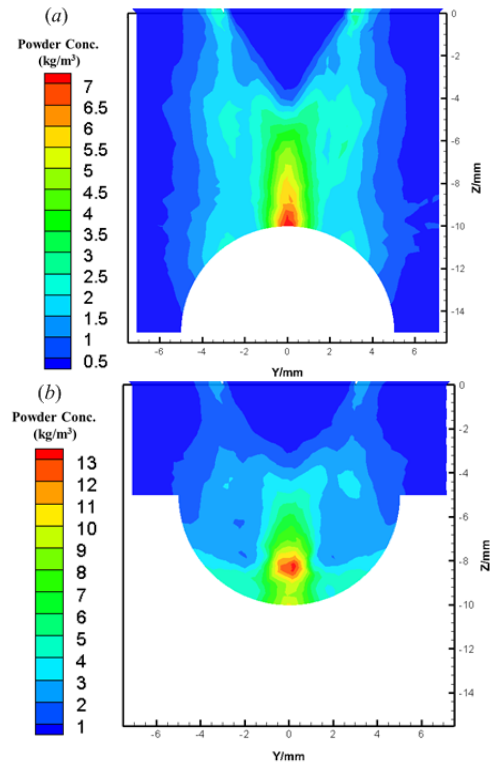

Fig. 14. The powder concentration distribution below the coaxial nozzle with cylindrical substrate of (a) convex surface or (b) concave surface.

4. CONCLUSIONS

It is important to deliver the powder particles to the deposition point in an optimal process parameters in coaxial laser cladding. Using the gas-solid model of a given coaxial nozzle proposed by this paper, it can be observed that the metallic powder flow converges from an annular distribution below the nozzle exit to a Gaussian distribution on the focus plane.

The effect of powder feeding parameters on the metallic powder flow has been investigated by the model. With the inner shielding gas rate increasing, the powder focal distance from nozzle exit increases and the maximum powder concentration decreases. The outer gas flow could improve the maximum concentration of powder flow without altering its focus. With the increase of carrier gas flow rate, the maximum powder concentration has a remarkable downward trend especially when the carrier gas rate increases from 3 m/s to 5 m/s. The maximum

powder concentration shows a strong positive linear relationship with the powder feed rate. The substrate and its shape have an important influence on the metallic powder flow by the means of changing the gas flow and bounce of the particles.

REFERENCES

Balu P., P. Leggett and R. Kovacevic (2012). Parametric study on a coaxial multi-material powder flow in laser-based powder deposition process. *J. Mater. Process. Tech.* 212(7), 1598-1610.

Dinda, G. P., A. K. Dasgupta and J. Mazumder (2012). Texture control during laser deposition of nickel-based superalloy, *Scripta Mater.* 67(5), 503-506.

Lin, J. (2000). Numerical simulation of the focused powder streams in coaxial laser cladding, *J. Mater. Process. Tech.* 105(1-2), 17-23.

Liu, H., X. L. He, Y. Gang, Z. B. Wang, S. X. Li, C. Y. Zheng and W. J. Ning (2015). Numerical simulation of powder transport behavior in laser cladding with coaxial powder feeding, *Sci. China-Phys. Mech. Astron.* 58(10), 104701.

Liu, J. C. and L. J. Li (2005). Effects of powder concentration distribution on fabrication of thin-wall parts in coaxial laser cladding, *Opt. Laser. Technol.* 37(4), 287-292.

Morsi, S. A. and A. J. Alexander (1972). An investigation of particle trajectories in two-phase flow systems. *J. Fluid. Mech.* 55(2), 193-208.

Pan, H. and F. Liou (2005). Numerical simulation of metallic powder flow in a coaxial nozzle for the laser aided deposition process, *J. Mater. Process. Tech.* 168(2), 230-244.

Pinkerton, A. J. (2007). An analytical model of beam attenuation and powder heating during coaxial laser direct metal deposition, *J. Phys. D: Appl. Phys.* 40(23), 7323-7334.

Pinkerton, A. J. and L. Li (2004). Modelling powder concentration distribution from a coaxial deposition nozzle for laser-based rapid tooling, *J. Manuf. Sci. E.-T. Asme.* 126(1), 33-41.

Tabernero, I., A. Lamikiz, E. Ukar, L. N. López de Lacalle, C. Angulo and G. Urbikain (2010). Numerical simulation and experimental validation of powder flux distribution in coaxial laser cladding, *J Mater Process Tech* 210(15), 2125-2134.

Yang, N. (2009). Concentration model based on movement model of powder flow in coaxial laser cladding. *Opt Laser Technol*, 41(1), 94-98.

Zekovic, S., R. Dwivedi and R. Kovacevic (2007), Numerical simulation and experimental investigation of gas–powder flow from radially symmetrical nozzles in laser-based direct metal deposition, *Int. J. Mach. Tool. Manu.* 47(1), 112-123.

Zhao, T., Z. Wang, M. Takei, K. Liu and Y. Cui (2015). Investigation of the dispersion behavior of inertial particles within accelerated domain, *J. Appl. Fluid. Mech.* 8(1), 103-112.